Available online at www.sciencedirect.com
SCIENCE DIRECT®
Composites Science and Technology 65 (2005) 2174–2188
COMPOSITES SCIENCE AND TECHNOLOGY
www.elsevier.com/locate/compscitech

Experimental methodology for high strain-rates tensile behaviour analysis of polymer matrix composites

J. Fitoussi [a], F. Meraghni [b,*], Z. Jendli [a], G. Hug [a], D. Baptiste [a]

[a] *LM3 UMR-CNRS 8006, ENSAM Paris, 151 bd de l'Hôpital 75013 Paris, France*
[b] *LPMM UMR-CNRS 7554, ENSAM Metz, 4 rue Augustin Fresnel Metz Technopôle 57070 Metz, France*

Received 24 August 2004; received in revised form 17 April 2005; accepted 1 May 2005
Available online 21 June 2005

Abstract

Material overall mechanical behaviour varies significantly under rapid straining as compared to quasi-static loading. Analysing the damaged elastic behaviour of composite materials under dynamic loading requires theoretical tools and experimental approaches integrating the strain rate effects. This work is concerned with development and optimisation of an experimental methodology devoted to the micro and macroscopic characterisation of composites mechanical behaviour under high-speed loadings. The applied experimental procedure has been optimised in an attempt to isolate the inherent inertial disturbances attributed to the test system. The optimisation aims at minimizing the amplitude of measurements perturbation in order to give rise to homogeneous stress/strain fields within the tested specimen. Using a servo-hydraulic machine, monotonic and interrupted tensile tests were performed at different strain rates and coupled to scanning electronic microscope observations. The developed approach has been applied at strain rates up to 200 s^{-1} for two composite materials: SMC-R26 and a woven carbon-epoxy laminate.
© 2005 Elsevier Ltd. All rights reserved.

Keywords: Damage mechanisms; Strain rate effects; High-speed tensile tests; Interrupted tensile test; SMC; Carbon-epoxy laminate; Dynamic behaviour

1. Introduction

Fibre reinforced polymer composites (FRPC) are very attractive for use in various engineering applications, notably those requiring service under dynamic loading conditions. While metals have been studied extensively over a wide range of strain rates, limited information is available with regard to the effects of strain rate on composites mechanical performances. Mechanical response of fibre reinforced polymer composites under low and high-speed loading is not well understood. This is one of the main aspects that inhibit their widespread use in the industry, although such composite materials are characterised by a high-energy dissipation. In fact, investigating dynamic behaviour of FRPC requires the development of an experimental methodology able to describe efficiently load-rate effects. Yet, experimental high-strain rate testing remains a difficult field and is full of complexities. Indeed, success with the high strain rate testing of polymer composites depends widely on the ability to isolate the inherent inertial disturbances attributed to the test system [1–6,8].

The primary objective of the present work is to set up and optimise an experimental approach aimed at characterising the mechanical behaviour of composite materials subjected to rapid loadings. The experimental methodology is built upon monotonic and interrupted

* Corresponding author. Tel.: +33 387 375 459; fax: +33 387 375 470.
E-mail address: Fodil.Meraghni@metz.ensam.fr (F. Meraghni).

0266-3538/$ - see front matter © 2005 Elsevier Ltd. All rights reserved.
doi:10.1016/j.compscitech.2005.05.001

rapid tensile tests and was coupled to microscopic observations using scanning electron microscope. Tensile tests were performed at different crosshead velocities yielding to strain rates from $\dot{\varepsilon} = 2 \times 10^{-4}\ s^{-1}$ (quasi-static) to $\dot{\varepsilon} = 200\ s^{-1}$. On the one hand, this study intended to quantify the strain-rate effects on the overall behaviour in terms of elastic properties, damage and ultimate characteristics. On the other hand, it contributes to investigate local processes involving damage initiation and growth.

Nevertheless, high-speed mechanical testing of polymer composites gives rise to specific difficulties due to inertial effects, non-uniform stress/strain distributions and measurements repeatability.

In fact, when a material is subjected to rapid accelerations many complex processes occur due to rapid straining coupled to inertial disturbances and damping attributed to the test system. The use of a servo-hydraulic test machine raises some issues related to the test control variables, notably for interrupted tests [7–10]. Due to the stress-wave propagation, the strain and the stress are non-uniform and hence the strain-rate can vary spatially and temporally into the tested specimen. To reduce this difficulty, numerical computations have led to an optimal design of the specimen geometry and the experimental damping systems have been optimised in terms of thickness and material. These simulations were achieved using ABAQUS finite element code [11] and are intended to model the stress wave propagation occurring for a high-speed tensile test. The developed experimental methodology is applied on two types of FRPC: a sheet moulding compound (SMC-R26) and a woven carbon-epoxy laminate.

2. Experimental methodology: procedure and testing devices

High-speed tensile tests have been conducted upon a servo-hydraulic test machine. As specified by the manufacturer (Schenck), the test machine can reach a crosshead speed range from 10^{-3} m/s (quasi-static) to 20 m/s. Moreover, the test force level is measured by a piezoelectric crystal load cell of a 50 kN capacity. It is worthy to note that strain rates have been estimated exclusively on the basis of strain gauge responses. To this goal, each specimen has been instrumented by a strain gauge positioned on its central zone. Tensile tests were carried out at different strain rates by using two experimental ways.

2.1. High-speed tensile tests until rupture

High-strain rate tensile tests were conducted using servo-hydraulic machine at different strain-rates until the composite specimen total failure. The test machine is equipped with a launching system. The composite specimen is positioned between the load cell (upper extremity) and the moving device (lower extremity) as sketched in Fig. 1. Prior to the contact between the sliding bar and the hydraulic jack, the latter one is accelerated over a straight displacement of 135 mm in order to reach the nominal crosshead velocity before the load begins. Once the contact occurs, the specimen is then subjected to a tension at a constant load-rate. The damping joint placed between the slide and the hydraulic jack may attenuate partially the wave effects caused by the dynamic shock.

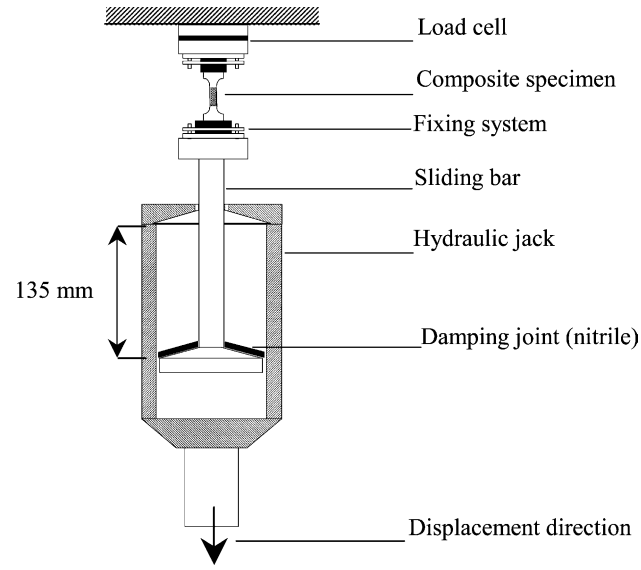

Fig. 1. Experimental device used for high-speed tensile tests until specimen rupture used on a servo-hydraulic machine.

2.2. Interrupted high-speed tensile tests

Interrupted tensile test technique has been applied to be able to monitor the progressive inflected damage as a function of the applied high-speed loading. The originality of this experimental methodology, proposed by Lataillade et al. [7], consists of the capability to interrupt the specimen loading at fixed stress levels. Indeed, due to inertial effects of the launching system, a rapid tensile test cannot be interrupted until the total failure of the specimen. Accordingly, the specimen is loaded simultaneously with a double-edge notched (DEN) fuse sample (Fig. 2) characterised by a brittle fracture. The fuse ligament width is assigned to a suitable level load to be reached when interrupting the loading of the specimen. The above brings about then a stress release in the specimen. This procedure is repeated several times onto the same specimen by changing the fuse (width) before each specimen undergoes a new reloading. One can hence reach a load level greater than the previous one.

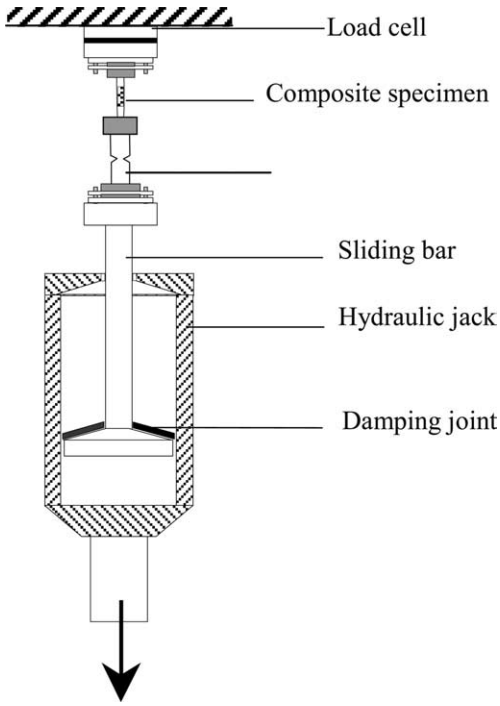

Fig. 2. Schematic diagram of the device used for interrupted high-speed tensile experiment.

3. Optimisation of high-speed tensile experiments

3.1. Methodology description applied to high speed tensile tests until rupture

As above pointed out, the transient loading nature coupled to the inertial effects due to rapid testing system generate a dynamic shock wave whose effects must be minimised. The damping joint inserted between the sliding bar and the tube of the hydraulic jack enables a partial absorption of the generated stress wave. Nevertheless, the damping joint must be able to attenuate the shock wave during its compression. Moreover, in order to ensure the derivation of the Young's modulus, the joint compression must be completely finished before the end of the complete elastic deformation of the specimen. It is obvious that it affects the loading rate. Consequently, an optimal design of the damping joint, in terms of constitutive material and geometry, may result in a constant strain-rate and in homogeneous strain and stress fields in the central zone of the composite specimen. For different crosshead velocities, several geometries and materials of the damping joint have been experimentally tested so that it gives rise to homogeneous strain/stress in the central zone of the composite specimen and may minimise the amplitude of the shock wave. This optimisation led to choose a damping joint consisting of a low impedance material: rubber nitrile (1.5 mm thickness). Furthermore, composite specimen geometry has been optimised as a result of numerical computations using ABAQUS finite element code. These simulations aimed at reducing the stress wave propagation occurring for a high-speed tensile test. The criterion used for the optimisation consists in reaching a stabilised strain distribution within the specimen gauge section at the beginning of the loading stage. The optimisation procedure relies upon coupling FE numerical results and experimental data. It falls into four stages (Fig. 3(a)):

(i) A tensile test is conducted at a fixed displacement-rate. The displacement induced at specimen extremities is measured. The damping joint, positioned between the sliding and the hydraulic jack, may limit the shock effect until its maximal compression corresponding to a rise time denoted hereafter (t_r). Its value lies in the range [2×10^{-4} to

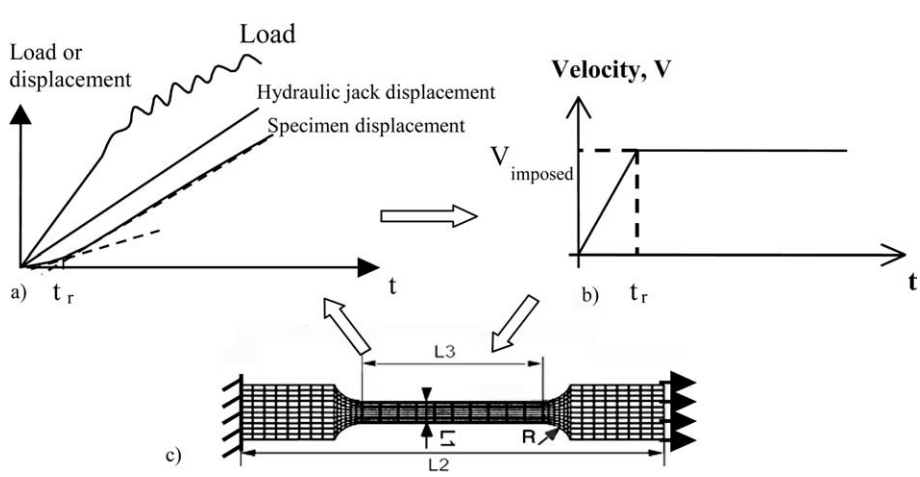

Fig. 3. Specimen optimisation stages coupling experimental tests and FE simulations. (a) Experimental data. (b) Boundary conditions. (c) FE computations for optimising the dumbbell-shaped specimen geometry.

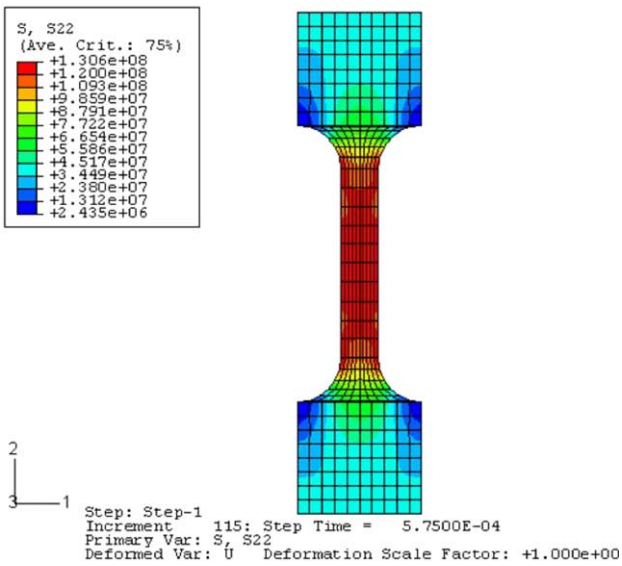

Fig. 4. Longitudinal tension stress (σ_{22}) distribution calculated for the optimised SMC specimen subjected to a tensile with an imposed load rate ($V = 1$ m/s, rise time $= 10^{-4}$ s).

10^{-6} s] and depends on the adopted joint thickness and the nominal test velocity. Beyond this time, the composite specimen is therefore subjected to a dynamic tensile loading. The first stage aims then at estimating experimentally the rise time (t_r).

(ii) Once the rise time evaluated, boundary conditions are numerically applied on the specimen extremities in terms of imposed velocity, according to Fig. 3(b), in order to compute the dynamic response of the specimen.

(iii) On the basis of the FE simulations and assuming that the specimen behaves like an elastic solid, a recursive optimisation procedure results in the determination of optimal geometrical parameters: L_1, L_2, L_3 and R. These parameters are those of a dumbbell-shaped specimen as sketched in Fig. 3(c) and are optimised in such a way of reducing the stress wave effects in the overall response and of generating homogeneous stress/strain field (Figs. 4 and 5).

(iv) Finally, high-speed tensile tests are achieved on the composite specimen to validate its optimised geometry. For both tested composite materials, the optimised specimens' geometries are summarised in Table 1.

In the case of the high speed tensile tests until rupture, the Table 1 gives the optimised specimen dimensions for two composites materials which have been studied. Further sections will illustrate the experimental results obtained when using these geometries.

Fig. 4 shows the longitudinal tension stress distribution predicted for the optimised SMC specimen subjected to an imposed velocity (1 m/s) leading to a theoretical value of strain-rate of $\dot{\varepsilon} = 33\ \mathrm{s}^{-1}$. The latter one is calculated on the basis of the imposed velocity, such as: ($\dot{\varepsilon}_{\mathrm{theoretical}} = V/l_3$). Furthermore, one can notice the homogeneity of the stress field in the centre of the specimen.

Fig. 5(a) shows the spatio-temporal profile of the longitudinal stress (σ_{22}) calculated along the central line of the SMC specimen. In this figure, one observes that the shock wave vanishes very quickly. Actually, the stress distribution becomes relatively homogeneous after 3.5×10^{-5} s and the stress value reaches homogeneously 1 MPa (corresponding to $\varepsilon = 7.33 \times 10^{-5}$). Moreover, in Fig. 6, one can note that after 10^{-4} s, the strain rate is also stabilised and has a rough value of 15 s^{-1}. As it will be illustrated in a following stage, the measured strain-rate value is much lower than the theoretical one (33 s^{-1}). This difference is due to the inertial effects of the gripping system.

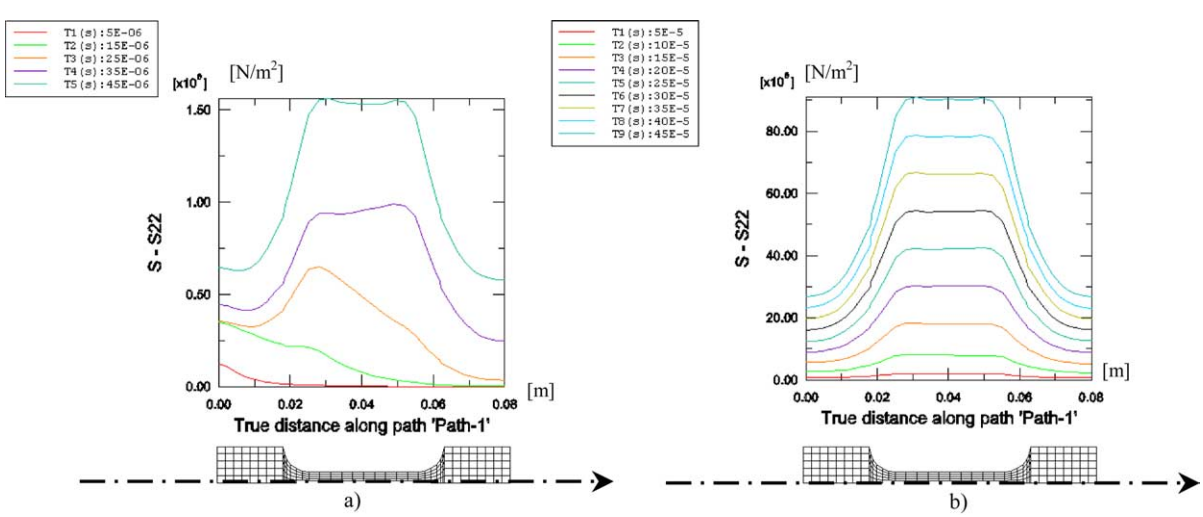

Fig. 5. Spatio-temporal profile of the longitudinal stress (σ_{22}) calculated along the central line of the SMC specimen. *Loading conditions*. Imposed velocity $V = 1$ m/s. (a) First steps and (b) next steps.

Table 1
Specimen dimensions optimised for both tested composite materials

	L_1 (mm)	L_2 (mm)	L_3 (mm)	R (mm)
SMC-R26	6	80	30	7
Carbon/epoxy woven laminate	6	80	15	7

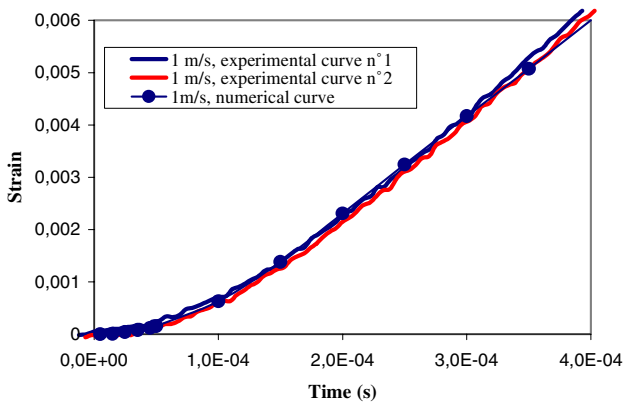

Fig. 6. Evolution of the strain in the central zone of the specimen. Comparison between experimental and numerical results obtained for the optimised geometry for SMC composites.

Beyond the rise time, the material is submitted to a homogeneous stress of about 7 MPa which corresponds to the first stages of the elastic behaviour. This will allow more accurate measurement of the Young's modulus without strain-rate variation and dependence.

On the basis of the good agreement between experimental curves obtained using the optimised geometry and numerical results, one can claim that the numerical analysis validates the proposed geometry. This geometry ensures the homogeneity of the stress/strain field (from a stress value of 1 MPa corresponding to a strain of 7.33×10^{-5}). Additionally, one can notice that a constant strain rate during the quasi-totality of the test (from a stress value of 7 MPa which corresponds to a strain of 6.28×10^{-4}).

Similar results have been obtained for the second material geometry of Table 1.

It should be pointed out that rectangular section tabbed end bars can also be used. Dimensions resulting from optimisation are $36 \times 6.5 \times 2.7$ mm^3 with a smaller central gauge zone of 16 mm long. This geometry is also adopted for the interrupted tensile tests. As shown in Figs. 7(a) and (b), the simulated results obtained for the bars also validate this second geometry. Indeed, the strain becomes rapidly homogeneous (from a stress of 7 MPa) whereas the strain rate is completely stabilised after 10^{-4} s and can reach a high value of 58 s^{-1} due to the small central gauge zone. In addition Fig. 7(b) compares the evolution of the strain for both geometries is the case of a tensile test performed at 1 ms^{-1}. These results confirm that this second geometry is validated too even if it presents a smaller gauge length.

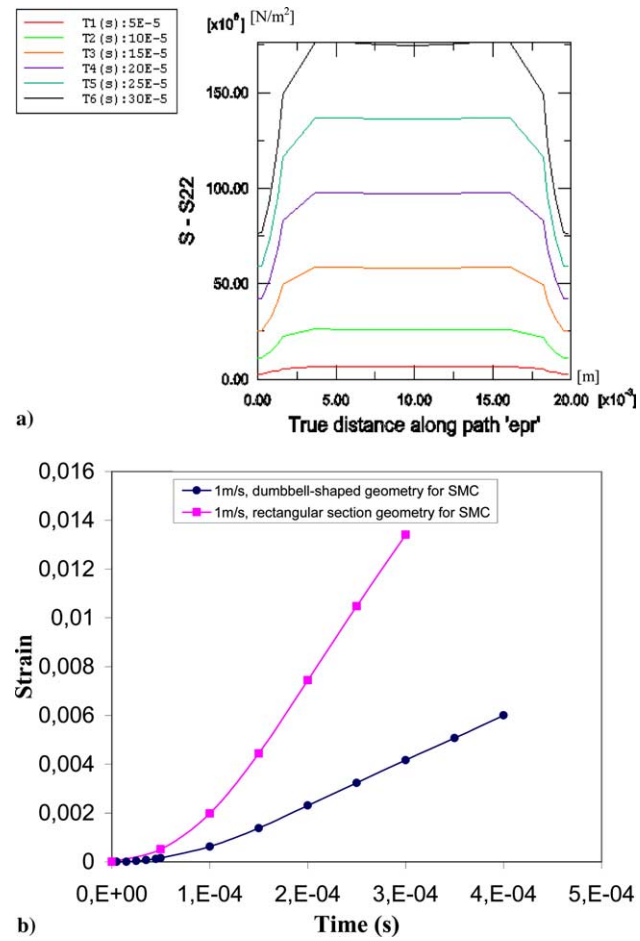

Fig. 7. Stress and strain evolution for a rectangular section tabbed end bars calculated for SMC composite. *Loading conditions*. Imposed velocity $V = 1$ m/s giving rise to a strain-rate of $\dot{\varepsilon} = 58$ s^{-1} (for the second geometry). (a) Spatio-temporal longitudinal stress distribution calculated along the specimen central line. (b) Strain evolution vs. time (comparison of two specimen geometries).

For interrupted high-speed tensile tests, the optimisation procedure is illustrated in the following sections. First, it aims at optimising the fuse and therefore the system consisting of the fuse sample in series with the composite specimen.

3.2. Optimisation and validation of the fuse geometry

For interrupted high-speed tensile tests, the load level reached prior to an elastic release is assigned to the fuse ligament width. Hence, a preliminary experimental analysis intends to characterise the evolution of the failure load as a function of the ligament width (W). This allows the determination of geometrical and mechanical parameters of the fuse sample. As aforementioned, the fuse must fail in a brittle manner and exhibit a linear elastic mechanical response consequently insensitive to the strain-rate. Several rapid tensile tests were conducted and have allowed the retention of a double notched fuse made of polymethylmethacrylate (PMMA). On the basis

of the expected load levels, the fuse samples are double notched bars of length 80 mm and 20 mm total width. For SMC composites, fuse thickness was 4 mm, whereas for the carbon/epoxy woven laminates, it was 6.5 mm (Fig. 8).

Fig. 9 shows the overall response of 4 mm thickness fuses having different ligament widths and subjected to tension at a crosshead speed of 1 m/s. One notices that, after a rise time of approximately 1.5×10^{-4} s, the dynamic response becomes linear until the maximum load reached prior to the brittle fracture. This rise time corresponds to the total compression of the damping joint.

These high-velocity tensile tests have contributed to establish experimentally the relationship between the interrupting load level and the fuse ligament width as illustrated in Table 2.

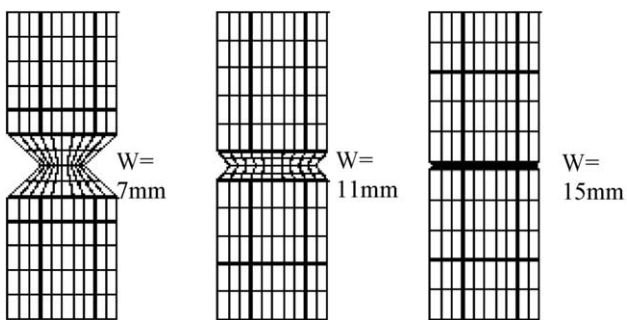

Fig. 8. PMMA double notched fuse geometry with different ligament widths and 4 mm thickness.

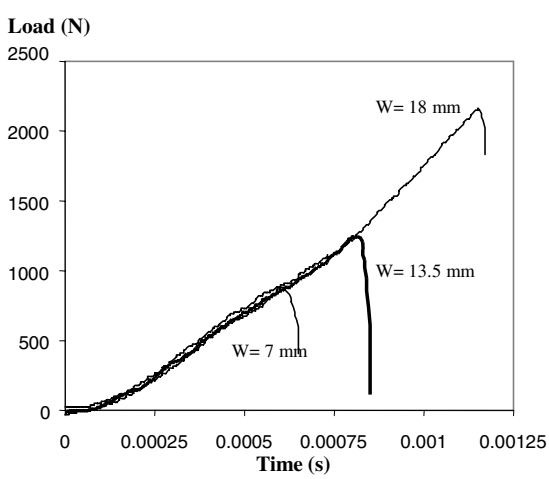

Fig. 9. Load vs. time curves for PMMA fuses having different ligament widths and subjected to tensile tests performed at 1 m/s crosshead displacement rate.

Using ABAQUS code, numerical simulations were carried out to assess the stress wave propagation involved into the fuse sample during high-velocity tensile tests. Boundary conditions applied for these numerical computations are those defined by experimental conditions and results. These are applied in terms of rise time ($t_r = 10^{-4}$ s), maximal velocity ($V_{max} = 1$ m/s). The PMMA fuse is clamped at upper end and subjected to a constrained displacement according to the velocity curve shown in Fig. 10 for example.

In what follows, numerical results for a velocity ($V_{max} = 1$ m/s) are presented for the fuse specimen with a ligament width $W = 7$ mm. Note that for other conditions, numerical simulations provide similar results.

Considering the different time increments, one notices that the front of longitudinal stress wave remains steady close to the fuse notch (Fig. 11). For the whole time steps, FE analysis shows that the stress front is not shifted along the fuse longitudinal line. In addition, the stress distributions, produced during the dynamic event, are numerically estimated along the fuse central line as well as along the ligament width. As reported by Figs. 11, these stress distributions exhibit a homothetic increase as a function of time increments. On the basis of these results, one can claim that, in terms of dispersion and perturbation, adopting these experimental conditions may minimise dynamic stress wave effects.

3.3. Optimisation and validation of the system: fuse in series with the composite specimen

The optimisation of the whole system was conducted according to the same stages described in Section 3. In what follows the composite specimen is clamped at the

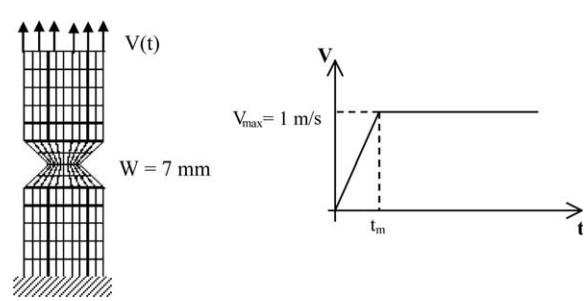

Fig. 10. The FE mesh and boundary conditions used in the modelling.

Table 2
Correlation between maximal load level and the ligament width of PMMA fuse

Ligament width (mm)	7	10.5	12	13.5	14.5	15	15.5	16
Maximal load (N)	822	1059	1089	1314	1511	1635	1721	1842

These load levels are estimated from tensile tests performed at 1 m/s crosshead velocity.

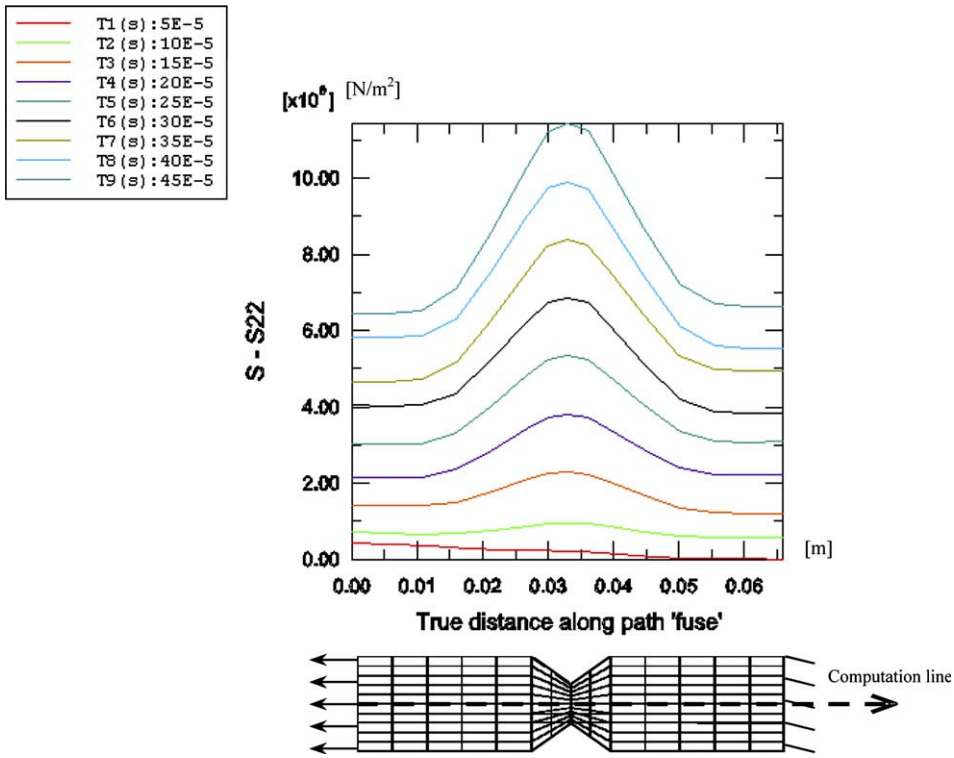

Fig. 11. Numerical predictions of the stress distributions along the fuse computation line (σ_{22}) estimated for different calculation steps ($W = 7$ mm).

upper extremity and is in series with the PMMA fuse. The junction between the specimen and the fuse is realised using a steel intermediate grip. The fuse is fixed to the sliding bar (lower extremity). Numerical computations are performed upon this system subjected to boundary conditions described in Section 3.1. These conditions consist of a velocity curve defined by a rise time ($t_r = 1.5 \times 10^{-4}$ s) and maximal velocity ($V_{max} =$ 1 m/s). The specimen, the fuse and the intermediate grip are assumed to behave elastic. SMC composite test specimens are rectangular section tabbed ends bars and having the dimensions of $36 \times 6.5 \times 2.7$ mm^3. The length of the central working zone is of about 16 mm. Tabs with tapered ends are bonded on each side of the specimen. These tabs allow a smoothed load introduction. They will reduce stress concentration and thus the shock wave stress effects. The adopted specimen geometry was chosen in order to carry out microscopic observations using a scanning electron microscope (SEM) after each interrupted high-speed tensile test. For the second composite material (carbon/epoxy), specimens adopted have a dumbbell-shaped geometry, with dimensions given in Table 1.

Fig. 12 shows an example of the stress distribution calculated for different load increments and represented along the central line of the whole system: fuse-composite specimen (SMC). One notices that the fuse exhibits stress profiles and levels similar to those optimised in Section 3.1. Furthermore, as reported in Figs. 12 and 13, one observes that the longitudinal stress profile increases progressively and remains uniform (from 2 MPa) along the specimen line whereas the strain rate is constant (about 13 s^{-1}) after a rise time of 2×10^{-4}s (corresponding to a tensile stress of about 7 MPa). The stabilised strain rate is of about 13 s^{-1}. Fig. 14 shows clearly the inertial effect due to the presence of the fuse and of the intermediate gripping device. It results in a strain rate decrease and an increase of the rise time. Hence, for the adopted experimental conditions one can claim that the dynamic stress wave does not generate parasite effects yielding to a premature damage or a failure of the tested specimen. These uniform stress distributions indicate that prior to the damage onset into the tested composite specimen the strain is spatially homogenous and the strain-rate may be constant from about 8 MPa corresponding to a time step of 4.5×10^{-4} s (Fig. 12). Simulated and experimental strain evolutions, obtained in the central point of the specimen, are in good agreement. Moreover, Fig. 15 shows that the stress and the strain increase simultaneously. No significant spatio-temporal gap is observed. Furthermore, this figure shows that the oscillations of the intermediate gripping device, beyond the failure of the fuse, may not cause additional damage due to the compression. In fact, the maximal compression

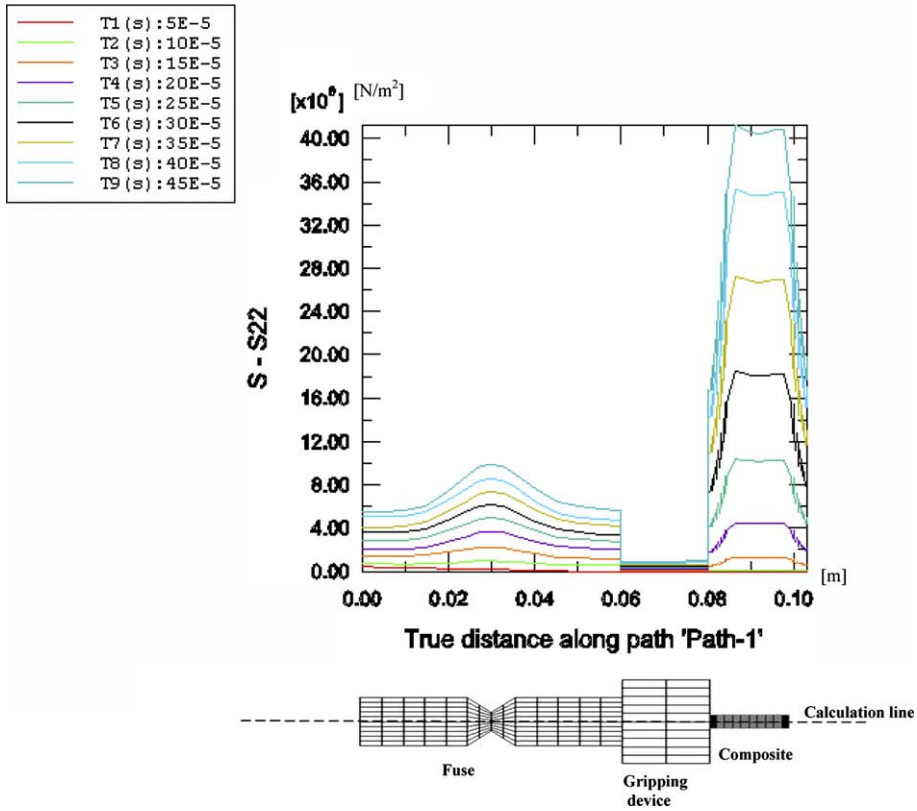

Fig. 12. Longitudinal stress (σ_{22}) profile calculated along the system fuse-specimen (SMC) line.

stress reached in the specimen does not exceed 80% of the tensile stress reached at the previous stage.

4. Experimental investigation and validations

The developed optimisation methodology based on experimental tests coupled to the numerical simulations was validated at strain rates up to 200 s^{-1} for two types of FRPC. These composite materials consist of a Sheet Moulding Compound (SMC-R26) and a woven carbon-epoxy laminate.

4.1. Materials descriptions

The first composite material is a Sheet Moulding Compound noted SMC-R26. It consists of an unsaturated polyester resin reinforced by glass fibres and weakly filled with calcium carbonate fillers ($CaCO_3$). Glass fibres have a weight content of 26% and are assembled in bundles in such a way that each one contains approximately 200 fibres. These bundles are randomly oriented in the material compression plane and have a constant length ($L = 25$ mm) with a fibre diameter of

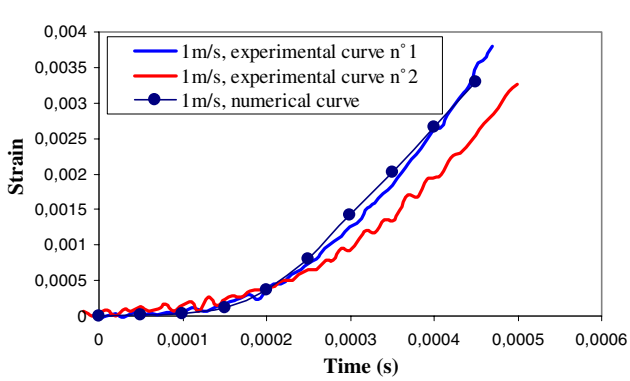

Fig. 13. Strain evolution vs. time: numerical and experimental results obtained in the central point of the SMC specimen submitted to an interrupted tensile test.

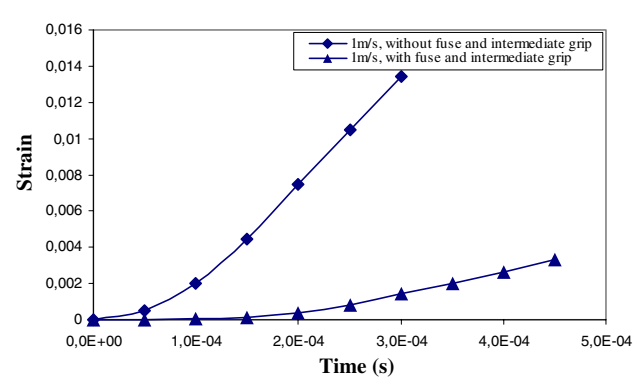

Fig. 14. Numerical strain evolution vs. time obtained in the central point of the SMC specimen, Inertial effect due to the presence of the fuse and the intermediate gripping device.

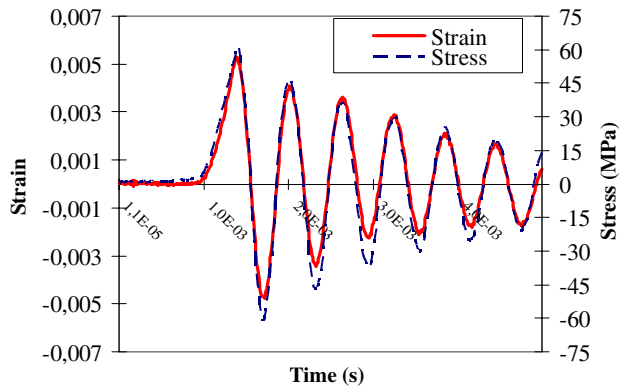

Fig. 15. Experimental strain and stress evolution vs. time measured during an interrupted tensile test.

15 μm. The random distribution of reinforcement confers to the material a microscopic heterogeneous aspect and an overall transverse isotropic mechanical behaviour. The SMC-R26 tested plates were prepared of thickness 2.7 mm and were cured at 140 °C with an applied pressure averaging between 7 and 8 MPa for 2 min [9,10].

The second composite material is a carbon-epoxy laminate. The latter is manufactured from a balanced woven fabric of HR carbon fibres. The weaving pattern is shown in Fig. 16. It is worth noting that there are five bundles oriented in both weaving directions: the warp and the fill direction.

The plies are impregnated by an epoxy matrix with a cure temperature of 175 °C. The tested composite is made of eight equally oriented plies resulting in a total thickness of approximately 2.5 mm. The overall carbon-fibre volume content of the laminate is 50.5%. As the material's properties in the two fibre orientations are identical, the mechanical behaviour of the composite can be considered as orthotropic with a quadratic symmetry. In this study, the tensile load has been applied at an angle 45° with respect to the orientation of the fibres (Fig. 17).

4.2. Effects of strain-rate on the overall tensile response

The application of the optimised methodology has contributed to an investigation into the sensitivity of the mechanical characteristics to the strain-rate, in terms

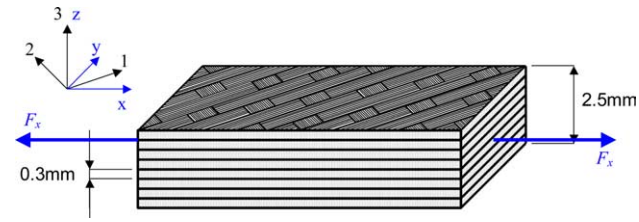

Fig. 17. 8-ply woven carbon-epoxy laminate. Tensile load applied at 45° with respect to the orientation of the fibres.

of the linear, non-linear behaviour and ultimate properties. These high-speed tensile tests were conducted for both studied materials at different strain-rates until the specimen completely fails. Note that for both investigated materials the strain rates have been determined directly on the basis of strain gauges temporal responses.

4.2.1. SMC-R26 composite material

For SMC-R26 composite, tested specimens are dumbbell-shaped and their dimensions are those resulting from the optimisation procedure and given in Table 1.

As shown in Fig. 18, stress–strain (σ–ε) tensile curves plotted for several strain rates show clearly that the overall behaviour is load-rate dependent. Indeed, under rapid tensile load SMC-R composites exhibit typically a non-linear response. The beginning of the non-linearity is noticed around 30% of the maximum loading. An inflection point, commonly called knee-point, characterises this kind of composite materials. Tensile tests were achieved at crosshead velocities from quasi-static to 9 m/s corresponding to strain rates from 10^{-3} to 150 s^{-1}. Fig. 18 shows that initial slopes of the stress–strain curves, estimated for a strain less than 0.3%, are roughly identical for the different tested strain rates. Therefore, it means that the elastic modulus remains insensitive to the load rate for the explored velocity range. It has a rough average value of 13 GPa. However, the microstructure variability of this class of materials [9,10,13–15] can bring about a slight discrepancy notably for dynamic loadings.

Additionally, Fig. 19 indicates that the non-linear stage of the overall response rises considerably as the strain rate increases. It is worth noting that the first non-linearity of the tensile curves corresponds to the

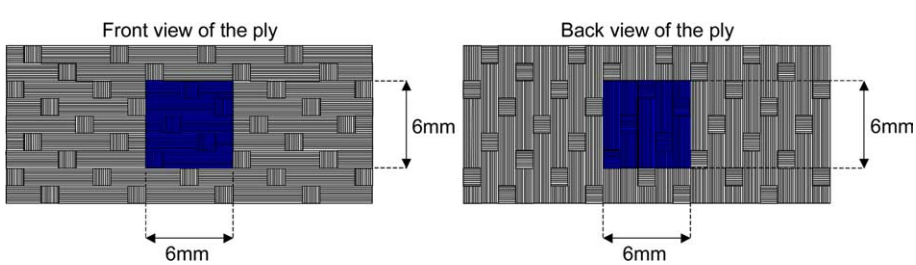

Fig. 16. Both views of the weaving pattern of each ply constituting the carbon-epoxy laminate.

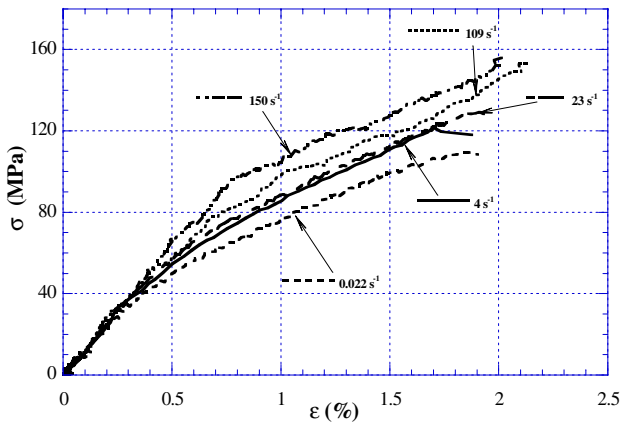

Fig. 18. Experimental strain–stress tensile curves for SMC-R26 composites obtained for tests carried out at strain rates: 0.022, 4, 23, 109 and 150 s^{-1}.

damage mechanisms initiation, which can be characterised by the damage threshold in terms of strain ($\varepsilon_{threshold}$) and stress ($\sigma_{threshold}$).

Furthermore, a mechanical behaviour accommodation is noticed for the high strain rates. The above arises through an increase of the ultimate strain and stress. Indeed, in terms of stress and strain, the ultimate properties and the damage threshold increase significantly for high strain rate. As illustrated in Fig. 19, one can see that the strain rate effect is more noticeable and marked on the ultimate stress than the strain.

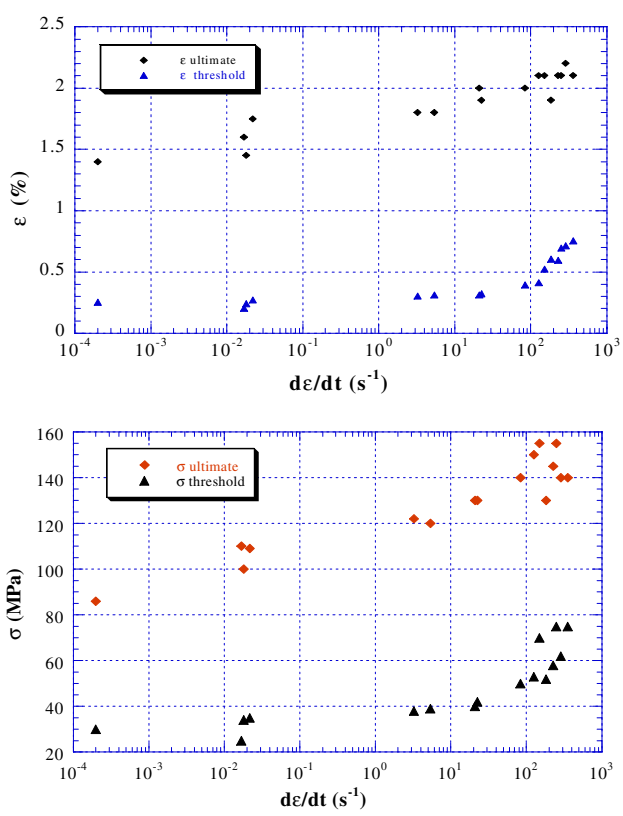

Fig. 19. Effects of strain-rate on the damage threshold and ultimate properties in terms of strain and stress (SMC-R26).

These experimental findings are consistent with those obtained in other works [1,2]. Their authors have pointed out that tensile strength increases with strain rate. In addition, one notes a shift of the damage initiation (corresponding to the first macroscopic non linearity) by increasing the strain rate. Actually, when varying the stain rate from the quasi-static to 250 s^{-1}, the stress damage threshold (corresponding to the first non linearity of the tensile curves) is delayed from 30 to 80 MPa (Fig. 19). While, the strain damage onset increases from 0.25% to 0.77%.

4.2.2. Woven fabric carbon-epoxy laminate

For this composite material, the tested specimens are dumbbell-shaped. Their geometry is the result of the previously described optimisation procedure whose dimensions are given in Table 1. The total longitudinal strain was measured by means of strain gauges. The experimental results obtained through high-velocity tensile tests until failure are comparable to those of the SMC-R26. In fact, stress–strain curves corresponding to tensile tests performed at strain-rates of 0.5, 25 and 60 s^{-1} show that the initial Young's modulus is insensitive to the load rate. Since the material is loaded at 45° with respect to the fibres orientation, its mechanical behaviour becomes strongly non-linear beyond the elastic stage, as shown in Fig. 20. Furthermore, as the stain-rate increases, the threshold of non-linear stress–strain behaviour increases significantly. This aspect brings about a behaviour accommodation that leads to an upward trend of the reached maximum stress.

4.3. Effects of strain-rate on the damage onset and kinetic

Interrupted high-speed tensile tests have widely contributed to evaluate the rate dependence of the damage in terms of initiation and growth for both investigated composites. Damage analysis was conducted according to two ways. The first intends to estimate the macroscopic Young's modulus reduction (D_{macro}) whereas the second aims at quantifying the damage accumulation (d_{micro}) at the microscopic material scale. Several works [9,10,14] focusing on damage in polymer reinforced fibre composites have been conducted using different experimental techniques such as acoustic emission [15], micrographs, C-Scan. They pointed out that composite materials fail through a sequence of damage mechanisms, namely: matrix microcracking, fibre-matrix debonding, interfacial decohesion and fibre breakage. The three first processes often instigate a progressive material degradation involving therefore a high-energy dissipation, whereas the last mechanism precedes the material collapse. Macroscopic damage

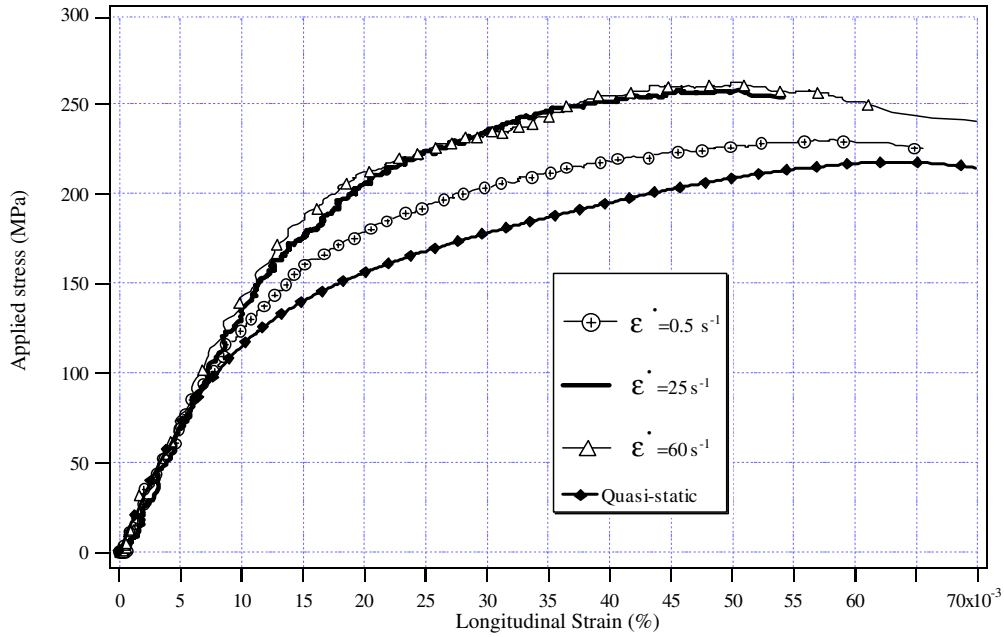

Fig. 20. Experimental strain–stress tensile curves for woven carbon/epoxy composite.

can be quantified by the tensile modulus reduction using the well-known damage mechanics [17]. The damage scalar parameter is thus expressed such as

$$D_{\text{macro}} = 1 - \frac{E^{\text{D}}}{E^{0}},$$

E^0 and E^{D}, are, respectively, the Young's modulus of virgin and damaged material. E^0 is determined by the initial slope of the stress–strain curve. The current modulus (E^{D}) is estimated by the slope of the reloading curve after each tensile test interruption at a predefined load level (Fig. 21).

Additionally, the local damage estimation aims at establishing a relationship between the micro-defects density, generated by the interface decohesions, and the macroscopic strain/stress applied level. After each interrupted tensile test, damage accumulation is investigated by means of SEM micrographs performed upon a representative element volume (REV). Specimen cartography is achieved using image-analysis. These contribute to characterizing the bundles degradation, in terms of matrix micro-cracks and fibre-matrix debonding which are the predominant microscopic damage mechanisms for composite material [15–18]. This investigation results in a quantitative damage evaluation by estimating defects effects. For that, one defines first a micromechanical damage parameter describing the debonded fibres content (f_{d}). The microscopic damage state can be represented at the local scale as

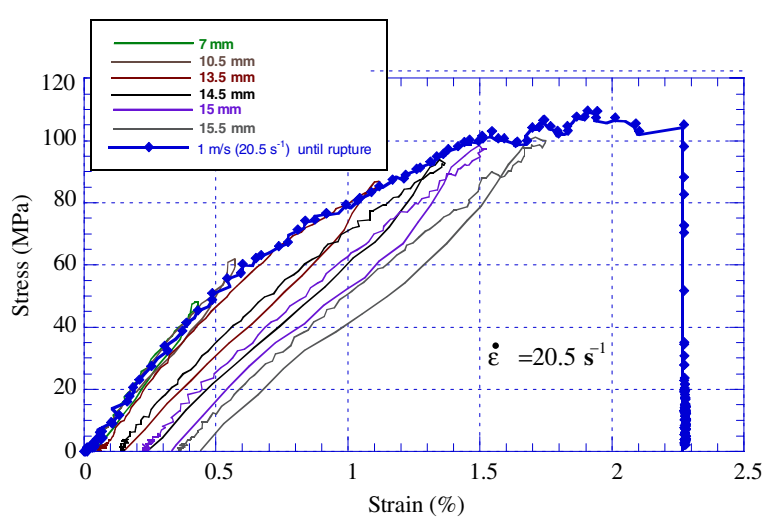

Fig. 21. Stress–strain curve obtained by performing interrupted tensile test at 20.5 s^{-1} (SMC-R26).

$$d_{\text{micro}} = \frac{f_{\text{d}}}{f_{\text{v}}},$$

where f_{d} is the volume fraction of debonded fibres and f_{v} is the fibre volume content in the REV. Microscopic observations have enabled to establish that damage growth in composites is mainly governed by the fibre-matrix debonding. Therefore the micromechanical damage (d_{micro}) can be considered as a damage indicator. This choice was adopted by several authors among them Lataillade et al. [7].

4.3.1. SMC-R26 composite material

Interrupted high-speed tensile tests have been achieved on SMC-R26 composite for the following strain rates: 0.0002, 3, 8 and 20.5 s^{-1}. These correspond, respectively, to crosshead velocities of 2×10^{-3}, 0.2, 0.5 and 1 m/s. SMC-R26 specimens are rectangular section tabbed ends bars. Dimensions resulting from the optimisation procedure are: $36 \times 6.5 \times 2.7$ mm^3.

As detailed in Section 2.2, the specimen is loaded in series with a brittle fuse (PMMA). By changing the fuse width, one can interrupt the high-speed test at a fixed load level. This procedure is repeated several times on the same specimen increasing the fuse width before each new re-loading. For each "unloading/re-loading" loop (Fig. 21), the evolution of the damage parameter (D_{macro}) is experimentally estimated.

As reported in Fig. 22, the evolution of the macroscopic damage parameter is plotted against the strain level for three tested strain rates. Experimental findings from interrupted tensile tests confirm that increasing the strain rate leads to a delayed macroscopic damage initiation. Indeed, for a strain rate of 3 s^{-1}, macroscopic degradation begins at a strain level of 0.25% when for a strain rate of 20.5 s^{-1}, the first stiffness reduction appears at a strain in the order of 0.43%. Hence, it easily follows that the damage evolution is relatively reduced as the crosshead rate increases from quasi-static to intermediate speed. Thus, one can claim that the stiffness reduction is rate dependent. However, the maximal critical value of D_{macro} does not seem to be rate dependent.

Besides the stiffness reduction analysis, a microscopic investigation was conducted to relate the micro-defects density and the macroscopic strain/stress applied level. This microscopic investigation is achieved by means of SEM micrographs performed upon a representative element volume (REV). It is worthy to note that the investigation zone is considered as representative of the material microstructure. In addition, microscopic observations have established that this zone is statistically representative for the damage accumulation. First stages of the damage are generated by the matrix micro-cracks leading to interface decohesions. Nevertheless, it must be emphasised that the micro-defects coalescence is increased for reinforcements having an orthogonal orientation with the maximum stress direction. However, it remains confined and limited for the fibres less oriented (Fig. 23).

Fig. 24 illustrates the accumulation of micro-defects, generated by the interface decohesions, as a function of the macroscopic strain level. One observes that at the local scale the damage growth is shifted in term of strain

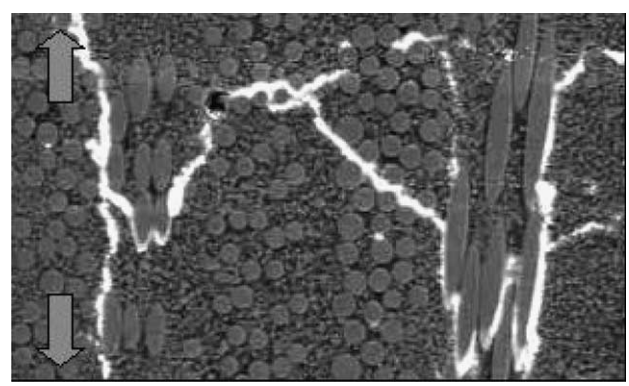

Fig. 23. *SEM observation*. Matrix micro cracks coalescence leading to interfacial decohesion (SMC-R26, $\dot{\varepsilon} = 20.5$ s^{-1}).

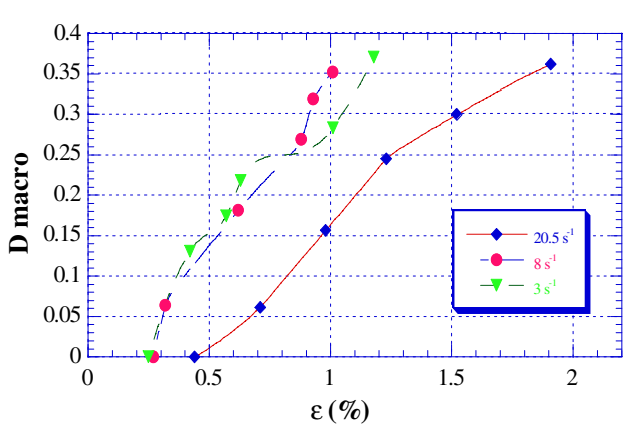

Fig. 22. Longitudinal Young's modulus reduction evolution vs. applied strain and plotted for different strain-rate (SMC-R26).

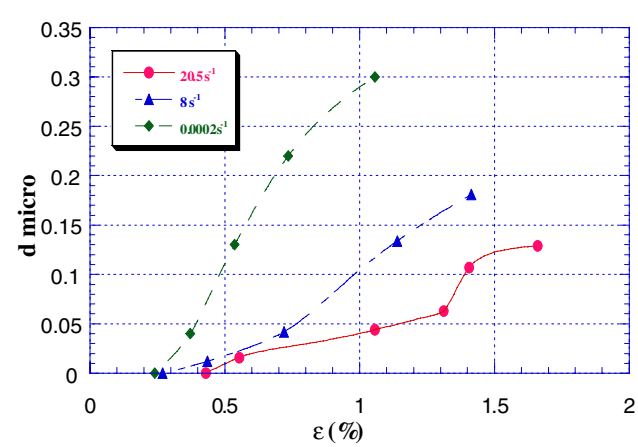

Fig. 24. Evolution of damage parameter (d_{micro}) vs. applied strain and plotted for different strain-rates (SMC-R26).

and exhibits a lessened growth kinetics due to the strain rate effect. Both aspects may be related to the viscous effect generated by the delay of the dissipation occurring at interfacial zones. Consequently, one notices a lag in the macroscopic damage initiation coupled to a slight decrease in term of its evolution.

4.3.2. Woven fabric carbon-epoxy laminates

For the carbon-epoxy laminate, the specimens used for the interrupted tests had the same geometry as those tested until failure. Interrupted tensile tests were performed at strain rates of 0.5, 25 and 60 s^{-1}. The apparent stiffness was taken at the beginning of each load cycle (Fig. 25) in order to determine the relative stiffness reduction. As expected, the obtained evolution of D_{macro} shows that, as the strain rate increases, the damage threshold is delayed in terms of strain (Fig. 26). Beyond this threshold, the damage evolution appears to be less sensitive to the strain rate. The parameter D_{macro} exhibits a comparable evolution for the three experimented strain-rates.

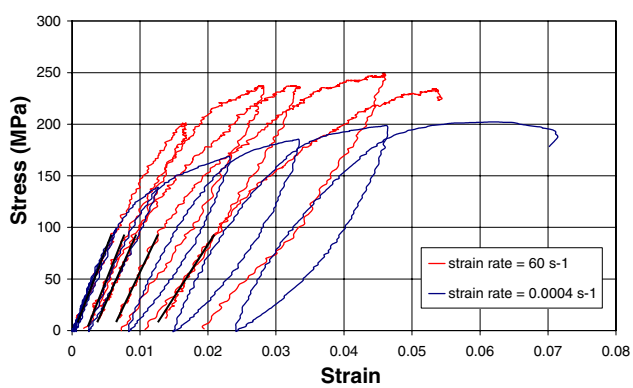

Fig. 25. Experimental curves with elastic releases for the second composite material: woven carbon/epoxy. The specimen is subjected to quasi-static and interrupted tensile tests at 60 s^{-1}.

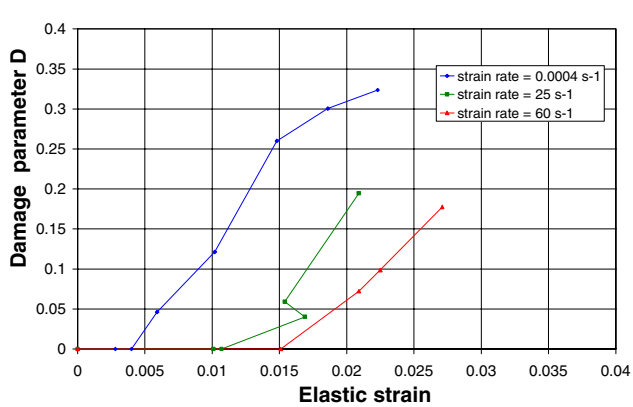

Fig. 26. Longitudinal Young's modulus reduction evolution vs. applied strain and plotted for different strain-rate. *Material*. Woven carbon/epoxy composite.

A qualitative microscopic analysis has yielded insights into the damage mechanisms involved in the material progressive degradation. It has been observed that for quasi-static loading, the damage onset occurs by matrix micro-cracking resulting in short cracks within the bundles close to the fibre-matrix interface. As the applied stress increases, these micro-cracks propagate through the matrix, but remain confined to the matrix zone between the fibres. They will therefore adopt the orientation of fibres: 45° with respect to the applied load (Fig. 27). When a propagating crack reaches the interface between two bundles, it will change its direction abruptly and continue its propagation following the interface between two plies. This phenomenon may lead to the onset of delamination.

For tensile tests performed at 60 s^{-1}, it has been observed that damage arises late in terms of strain level. Moreover, for rapid tensile tests, the accumulation of micro-cracks leads to a prompt damage localisation requiring hence a high-energy dissipation. This aspect might at least partly explain the slightly reduced damage kinetics at higher strain rates. It should be pointed out that, for similar strain levels (4.6% and 4.9%), damage remains diffuse under quasi-static tension (Fig. 28) whereas, as shown in Fig. 29, a damage localisation is observed under rapid loading conditions, just before the overall failure occurs [12,13].

5. Conclusion

The use of a servo-hydraulic test machine for dynamic loadings raises some issues related to the test control variables. The present work has proved that servo-hydraulic testing machine may be suitable to examine strain-rate effects on overall composite behaviour for moderate rates up to 200 s^{-1}. Nevertheless, success with the high strain rate testing of polymer

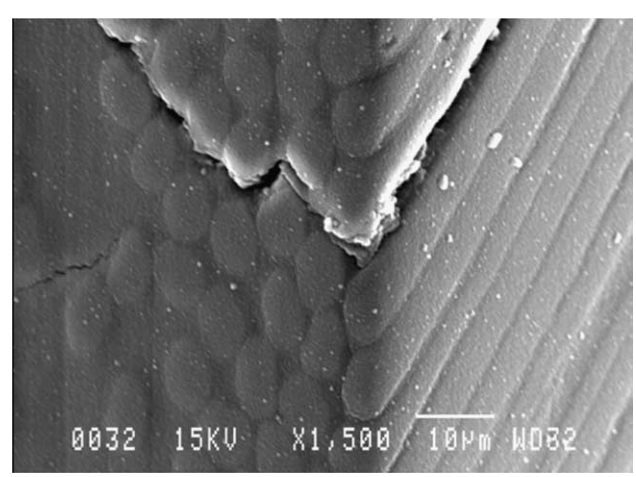

Fig. 27. Crack orientation in the woven carbon/epoxy composite.

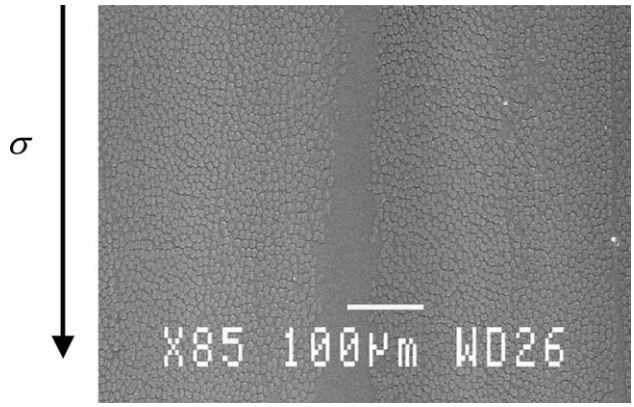

Fig. 28. SEM observation of the woven carbon/epoxy specimen subjected to a quasi-static tension. For an applied strain of 4.9%, damage remains diffuse and confined. It occurs mainly by matrix micro-cracking and interfacial debonding inside a bundle.

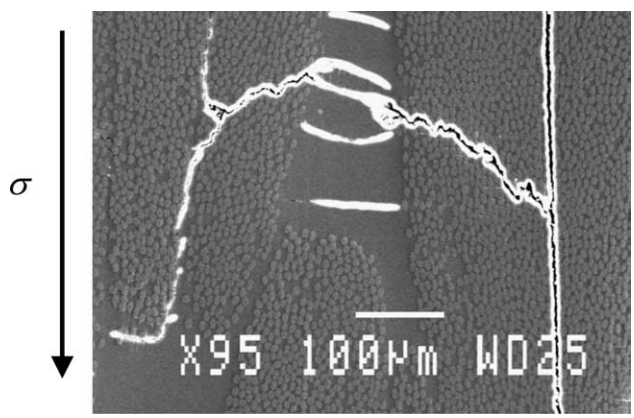

Fig. 29. SEM observation of the woven carbon/epoxy specimen subjected to a tensile test at $25\,s^{-1}$. For an applied strain of 4.6%, damage localisation occurs after the accumulation of matrix micro-cracks and coalescence between bundles.

composites requires an experimental methodology able to isolate inertial disturbances attributed to the test system. To this end, an experimental methodology has been developed and optimised. It aims at minimizing the amplitude of measurements perturbation for giving rise to homogeneous stress/strain fields within the tested specimen. Experimental findings, obtained from monotonic and interrupted tensile tests performed at different strain rate, were input in numerical computations using ABAQUS FE code for optimising iteratively the experimental conditions. The analysis of the stress wave propagation occurring for a high-speed tensile test has resulted in an optimal design of the specimen geometry and the experimental damping system: thickness and material characteristics. On one hand, the optimisation has contributed to generate uniform strain and stress fields yielding hence to a strain-rate spatially constant into the tested specimen. On the other hand, it has enabled a method for the interrupted high-speed tensile tests. These have provided the monitoring of the stiffness reduction evolution and the damage accumulation by interrupting the test at predefined load levels.

The developed experimental methodology based on dynamic tensile tests has contributed to emphasise the strain rate effects on the overall behaviour of SMC-R26 and carbon/epoxy woven laminate composites. As the strain rate increased, noticeable effects consist of a delayed damage onset followed by a slightly reduced damage accumulation. It was established that the strain rate brings about a viscous nature of damage evolution leading hence to the notion of the visco-damaged behaviour, which characterises both tested composite materials. Due to the time-dependent damaged-behaviour, the interface strengths are increased. That can explain readily the accommodation exhibited at the macroscopic scale. As the strain rate increases, the damage viscosity reduces then the degradation and its kinetics. For the carbon/epoxy laminate a rapid tensile test brings about a damage localisation requiring a high-energy dissipation delaying therefore the macroscopic specimen failure notably in terms of ultimate stress. The optimised experimental methodology will provide the experimental framework to validate a multi-scale model integrating the material microstructure effects. This model is currently developed and will be implemented into a FE code. It will be applied as a simulation tool and also as an inverse approach for optimising of composite choc components and structure on the basis of design requirements and material constitution.

References

[1] Okoli OI, Smith GF. High strain rate characterization of a glass/epoxy composite. J Compos Technol Res JCTRER 2000;22(1):3–11.
[2] Okoli OI. The effects of strain rate and failure modes on the failure energy of fibre reinforced composites. Compos Struct 2001;54:299–303.
[3] Harding J, Welsh LM. A tensile testing technique for fibre-reinforced composites at impact rates of strain. J Mater Sci 1983;18:1810–26.
[4] Rodney J Clifton. Response of materials under dynamic loading. Int J Solids Struct 2000;37:105–13.
[5] Dear JP, Brown SA. Impact damage in reinforced polymeric materials. Composites Part A Appl Sci Manufac 2003;34:411–420.
[6] Hsiao HM, Daniel IM. Strain rate behavior of composite materials. Composites Part B 1998;29B:521–33.
[7] Lataillade J-L, Delaet M, Collombet F, Wolff C. Effects of the intralaminar shear loading rate on the damage of multi-ply composites. Int J Impact Engng 1996;18(6):679–99.
[8] Pardo S, Baptiste D, Décobert F, Fitoussi J, Joannic R. Tensile dynamic behaviour of a quasi-unidirectional E-glass/polyester composite. Compos Sci Technol 2002;62(4):579–84.
[9] Jendli Z, Meraghni F, Fitoussi J, Baptiste D. Micromechanical analysis of strain rate effect on damage evolution in sheet molding

compound composites. Composites Part A: Appl Sci Manufac 2004;35(5):779–85.
[10] Jendli Z, Fitoussi J, Meraghni F, Baptiste D. Anisotropic strain rate effects on fibre-matrix interface decohesion in sheet moulding compound composites. Compos Sci Technol 2005; 65(3–4):387–93.
[11] HKS Inc, ABAQUS Theory and Users Manuals V. 6.2.1; 2001.
[12] Hug G, Baptiste D, Fitoussi J, Thévenet P. Analyse de l'endommagement dans les stratifies carbone/époxyde soumis à un chargement de traction à vitesse élevée. C R des JNC13-AMAC, Strasbourg, mars; 2003 [in French].
[13] Hochard C, Charles J-P. Endommagement de composites stratifiés carbone/époxy constitués de plis tissés'', Comptes rendus des JNC12-AMAC, Cachan; 2000. p.745–54 [in French].
[14] Mandell JF. Fatigue behaviour of Short Fiber Composite Materials. Compos Mater Ser ''Fatigue Compos Mater'' 1991;4:231–337.
[15] Meraghni F, Desrumaux F, Benzeggagh ML. Implementation of a constitutive micromechanical model for damage analysis in glass mat reinforced composites structures. Compos Sci Technol 2002;62:2087–97.
[16] Karjcinovic D. Selection of damage parameter – Art or science? Mech Mater 1998;28:165–79.
[17] Krajcinovic D, Mastilovic S. Some fundamental issues of damage mechanics. Mech Mater 1995;21:217–30.
[18] Fitoussi J, Guo G, Baptiste D. A statistical micromechanical model of anisotropic damage for S.M.C. Compos Sci Technol 1998;58(5):759–63.